JCB Journal of Cell Biology

ARTICLE

m^{6}Am methyltransferase PCIF1 negatively regulates ciliation by inhibiting BICD2 expression

Shanshan Xie[1*], Wenjun Kuang[2*], Mengzhe Guo[3*], Feng Yang[1*], Hao Jin[4], Xiying Chen[4], Li Yi[4], Chunxiao Huo[4], Zhangqi Xu[1], Aifu Lin[5], Wei Liu[6], Jianhua Mao[1], Qiang Shu[1], and Tianhua Zhou[4]

N6, 2′-O-dimethyladenosine (m^{6}Am) is a widespread RNA modification catalyzed by the methyltransferase PCIF1 (phosphorylated CTD interacting factor 1). Despite its prevalence, the biological functions of m^{6}Am in RNA remain largely elusive. Here, we report a critical role of PCIF1-dependent m^{6}Am RNA modification in ciliogenesis in RPE-1 cells. Our findings demonstrate that PCIF1 acts as a negative regulator of ciliation through its m^{6}Am methyltransferase activity. A quantitative proteomic analysis identifies BICD2 as a downstream target of PCIF1, with PCIF1 depletion resulting in a significant increase in BICD2 levels. BICD2 depletion leads to a significant reduction in ciliation. Crucially, the ciliary phenotype in PCIF1-depleted cells is reversed upon BICD2 knockdown. Further investigations reveal that PCIF1 regulates BICD2 protein levels through its m^{6}Am catalytic activity, which reduces the stability and translation efficiency of *BICD2* mRNA. Single-base resolution LC-MS analysis identifies the m^{6}Am site on *BICD2* mRNA modified by PCIF1. These findings establish the essential involvement of PCIF1-dependent m^{6}Am modification in ciliogenesis.

Introduction

N^6, 2′-O-dimethyladenosine (m^{6}Am) is an evolutionarily conserved mRNA modification located at the transcription start site of capped mRNAs and adjacent to the cap structure (Keith et al., 1978; Wei et al., 1975; Cowling, 2019). The methyltransferase PCIF1 (phosphorylated carboxyl-terminal domain interacting factor 1) has been identified as the specific methyltransferase responsible for the terminal m^{6}Am of mRNAs, influencing mRNA stability and cap-dependent translation (Akichika et al., 2019; Boulias et al., 2019; Sendinc et al., 2019; Sun et al., 2019). While complete loss of *Pcif1* in mice does not impact viability or fertility, *Pcif1* knockout mice exhibited a reduction in body weight (Pandey et al., 2020). Our previous work and other groups found that m^{6}Am and PCIF1 were involved in regulating gastric and colorectal tumorigenesis (Zhuo et al., 2022; Wang et al., 2023). Additionally, PCIF1 is involved in the modulation of vesicular stomatitis virus infection, HIV infection, and SARS-CoV-2 susceptibility (Tartell et al., 2021; Zhang et al., 2021a, 2021b; Wang et al., 2023). However, the physiological significance of m^{6}Am RNA modification remains largely unclear.

Primary cilia are microtubule-based organelles extending from the basal body in most mammalian cell types (Anvarian et al., 2019). They function as sensors of chemical and physical cues in the extracellular environment, regulating a variety of cellular and developmental processes (Nachury and Mick, 2019). Dysfunction of cilia due to genetic mutations or environmental factors leads to a range of human diseases known as ciliopathies, including primary ciliary dyskinesia and polycystic kidney disease (Reiter and Leroux, 2017). The m^{6}A (N6-methyladenosine) demethylase FTO (fat mass and obesity-associated protein) has been implicated in regulating motile ciliogenesis by demethylating *FOXJ1* (forkhead box protein J1) mRNA (Kim et al., 2021). Our previous work demonstrated that the m^{1}A demethylase ALKBH3 significantly inhibits non-motile ciliogenesis through the removal of m^{1}A sites on *Aurora A* mRNA (Kuang et al., 2022). However, the role of m^{6}Am modification in the formation of primary cilia remains unknown.

The BICD2 protein, also known as Bicaudal D homolog 2, plays a pivotal role in intracellular transport processes within eukaryotic cells (Suter et al., 1989; Hoogenraad et al., 2001, 2003; Huynh and Vale, 2017; Schlager et al., 2014). As a key adaptor protein, it connects the dynein motor complex to various cellular cargoes, facilitating their movement along microtubules toward

[1]Children's Hospital, National Clinical Research Center for Child Health, Zhejiang University School of Medicine, Hangzhou, China; [2]International Institutes of Medicine, The Fourth Affiliated Hospital, Zhejiang University School of Medicine, Yiwu, China; [3]School of Pharmacy, Xuzhou Medical University, Xuzhou, China; [4]Department of Cell Biology, Zhejiang University School of Medicine, Hangzhou, China; [5]MOE Laboratory of Biosystem Homeostasis and Protection, College of Life Sciences, Zhejiang University, Hangzhou, China; [6]Metabolic Medicine Center, International Institutes of Medicine and the Fourth Affiliated Hospital, Zhejiang University School of Medicine, Yiwu, China.

*S. Xie, W. Kuang, M. Guo, and F. Yang contributed equally to this paper. Correspondence to Shanshan Xie: sxie@zju.edu.cn; Tianhua Zhou: tzhou@zju.edu.cn.

the minus ends. BICD2's interaction with the small GTPase Rab6 enables it to participate in the recruitment of the dynein motor to Rab6-positive membranes in the Golgi apparatus and cytoplasmic vesicles (Matanis et al., 2002; Short et al., 2002; Reck-Peterson et al., 2018).

In this study, we reveal that PCIF1 negatively modulates ciliogenesis in mammalian cells through its catalytic activity. PCIF1 modifies the m^{6}Am site on *BICD2* mRNA, promoting the degradation and inhibition of translation of *BICD2* mRNA, thereby attenuating ciliation. Our data highlight the significance of the PCIF1-BICD2 axis in ciliogenesis through an m^{6}Am RNA modification-dependent mechanism.

Results

Depletion of *pcif1* promotes ciliation in mammalian cells

To elucidate the biological role of m^{6}Am in ciliogenesis, we employed two distinct small interfering RNAs (siRNAs) targeting the m^{6}Am methyltransferase PCIF1 in human retinal pigmented epithelial 1 (RPE-1) cells. Immunofluorescence experiments revealed a marked increase in the percentage of ciliated cells following PCIF1 knockdown (Fig. 1, A–D), a phenomenon significantly rescued by the ectopic expression of PCIF1 (Fig. 1, E–G). Furthermore, serum starvation, a condition known to induce ciliation in cultured cells, provided additional validation of PCIF1's inhibitory role in ciliogenesis, as the exogenous expression of PCIF1 significantly impeded ciliation under serum-starvation conditions (Fig. 1, H–K). These findings collectively signify that PCIF1 functions as a negative regulator of cilia formation in RPE-1 cells.

PCIF1 suppresses ciliogenesis in an m^{6}Am-dependent manner

To interrogate whether the m^{6}Am catalytic activity of PCIF1 underscores its role in ciliogenesis, we utilized a catalytically inactive mutant of PCIF1, incorporating an Asn553→Ala substitution in the NPPF motif, rendering it incapable of m^{6}Am modification (Akichika et al., 2019). Subsequently, we conducted rescue experiments by reintroducing either the wild-type or PCIF1-N553A variant into PCIF1-depleted RPE-1 cells. The rescue experiments unequivocally demonstrated that wild-type PCIF1, but not the PCIF1-N553A mutant, significantly rectified the ciliary defects in PCIF1-depleted cells (Fig. 2, A–C). Furthermore, the overexpression of wild-type PCIF1 impeded ciliogenesis, whereas overexpression of the PCIF1-N553A mutant showed no discernible effect under serum starvation conditions (Fig. 2, D–F). These findings collectively signify that the m^{6}Am methyltransferase PCIF1 inhibits ciliogenesis in a manner contingent on its m^{6}Am-dependent catalytic activity in mammalian cells.

PCIF1 inhibits ciliation through suppression of BICD2 expression

In light of our observation that PCIF1 negatively regulates the expression of the target protein (Zhuo et al., 2022), we conducted a thorough investigation into the underlying mechanism by employing tandem mass tag (TMT)-based quantitative proteomics in RPE-1 cells to elucidate how PCIF1 contributes to ciliation attenuation. The single knockdown experiment on cells was replicated in three independent experiments for TMT proteomics analysis. We comprehensively analyzed the proteomics data (Table S1) and identified 41 significantly upregulated hits (Fold Change >1.5, P value <0.05) between siPCIF1-1 and its control (Table S2), along with 14 significant upregulated hits (Fold Change >1.5, P value <0.05) between siPCIF1-2 and its control (Table S3). As a result, we identified 11 upregulated proteins in RPE-1 cells treated with either siPCIF-1 or siPCIF1-2 (Fig. 3, A and B).

Given their upregulation in PCIF1-depleted cells and the negative regulatory role of PCIF1 in ciliation, we hypothesized that downstream targets of PCIF1 should have the potential to promote ciliogenesis. As a logical extension of our investigation, we initiated immunofluorescence experiments to delineate the role of these eleven upregulated proteins in ciliogenesis. Among them, only BICD2 exhibited a significant effect on ciliation (Fig. 3, C–F; and Figs. S1 and S2). To further investigate the role of BICD2 in ciliogenesis, we conducted immunostaining experiments in cells overexpressing BICD2, revealing a significant promotion of ciliogenesis (Fig. 3, G–I). Importantly, rescue experiments showed that depletion of BICD2 significantly reversed the enhanced ciliation induced by PCIF1 knockdown (Fig. 3, J–L), implying that PCIF1 inhibits ciliation through the inhibition of BICD2 expression.

Depletion of PCIF1 increases the stability and translation of *BICD2* mRNA

Subsequently, we investigated whether PCIF1 modulates the protein level of BICD2 through its m^{6}Am catalytic activity. Western blot analysis revealed a noticeable elevation of BICD2 in PCIF1-depleted cells (Fig. 4 A), a phenomenon rescued by the ectopic expression of wild-type PCIF1 but not by PCIF1-N553A mutants (Fig. 4 B). These findings suggest that PCIF1 inhibits BICD2 expression through its m^{6}Am catalytic activity. We further explored the impact of PCIF1 depletion on the expression of *BICD2* mRNA. Quantitative real-time PCR (qRT-PCR) analysis demonstrated a significant increase in *BICD2* mRNA levels upon silencing of PCIF1 in RPE-1 cells (Fig. 4, C and D).

Given the known involvement of m^{6}Am in mRNA stability and translation regulation, we hypothesized that PCIF1 might regulate the expression of BICD2 by affecting the stability or translation of *BICD2* mRNA. mRNA decay assay revealed that the decay rate of *BICD2* mRNA was significantly reduced in cells depleted of PCIF1 when the transcription was halted with actinomycin D in RPE-1 cells (Fig. 4, E and F). Furthermore, polysome profiling analysis demonstrated that PCIF1 knockdown resulted in increased *BICD2* mRNA abundance in high-molecular-weight polysome fractions, indicative of high translation efficiency (Fig. 4 G). Collectively, these data indicate that PCIF1 plays a negative regulatory role in both the stability and translation of *BICD2* mRNA.

PCIF1 modifies *BICD2* mRNA with m^{6}Am sites

In light of PCIF1's role in suppressing ciliation through the downregulation of BICD2 expression, and recognizing that PCIF1's impact on ciliogenesis hinges, in part, on its m^{6}Am methyltransferase activity, we postulated the presence of m^{6}Am

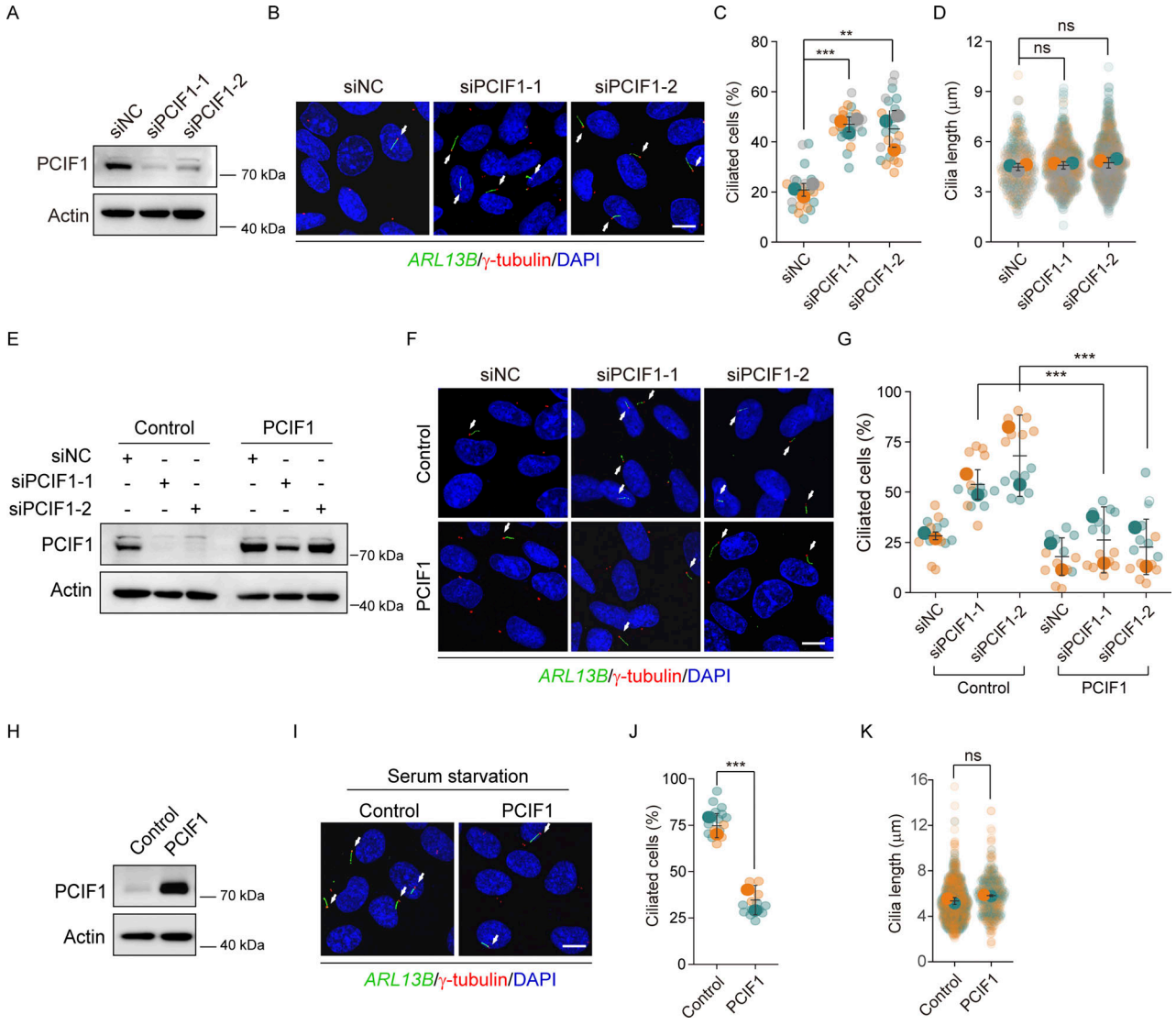

Figure 1. **PCIF1 suppresses ciliogenesis in RPE-1 cells. (A–D)** RPE-1 cells were treated with control or PCIF1 siRNAs for 48 h under normal culture conditions (DMEM/F12 supplemented with 10% FBS) and then applied for Western blotting or immunofluorescence analysis. **(E–G)** RPE-1 cells treated with the indicated siRNAs for 24 h were transfected with control or PCIF1 plasmid for another 36 h under normal culture conditions and then subjected to Western analysis or immunofluorescence. **(H–K)** RPE-1 cells transfected with the indicated plasmids for 48 h were treated with serum starvation for another 24 h and then applied for western analysis or immunofluorescence. Western blotting analysis of PCIF1 protein (A, E, and H). Actin is the internal control. Immunofluorescence images of RPE-1 cells with anti-ARL13B (green) and γ-tubulin (red) antibodies (B, F, and I). DNA was stained with DAPI (blue). Cilia were indicated by white arrows. Scale bar, 10 μm. Quantification of the percentage of ciliated cells (C, G, and J). Cilia length is measured by ImageJ (D and K). Quantitative analyses are depicted in SuperPlots, with each color representing an independent biological replicate. In the SuperPlots, smaller symbols indicate the ciliation percentage for each field of view or the cilia length of individual cells, while larger symbols represent the mean value calculated for each replicate. All error bars represent means ± SD. Student's *t* test, **P < 0.01, ***P < 0.001, ns, not significant. Source data are available for this figure: SourceData F1.

sites on *BICD2* mRNA. To precisely identify the m^{6}Am site on *BICD2* mRNA, we employed a single-base resolution method for targeted m^{6}A and m^{6}Am detection based on liquid chromatography-tandem mass spectrometry (LC-MS/MS) (Fig. 5 A). The results revealed distinct molecular weight differences of 14 or 28 Da in the fragments containing m^{6}A or m^{6}Am, respectively, indicative of the specific modification at this site (Fig. 5, B–E). Our LC-MS/MS analysis achieved the identification of the m^{6}Am site on *BICD2* mRNA with single-base resolution. Notably, we observed a noteworthy decrease in the signal abundance of RNA fragments containing m^{6}Am, as depicted in the total ion flow (TIC) diagram following PCIF1 knockdown (Fig. 5 F), while the signal abundance of RNA fragments containing m^{6}A remained unaltered (Fig. 5 G), demonstrating the sensitivity of detection of m^{6}Am modification at this site.

Knockdown of PCIF1 induces cell cycle arrest by enhancing ciliation

Primary cilia represent dynamic organelles intricately linked to cell cycle progression, with their assembly and disassembly tightly regulated (Kasahara and Inagaki, 2021). To investigate

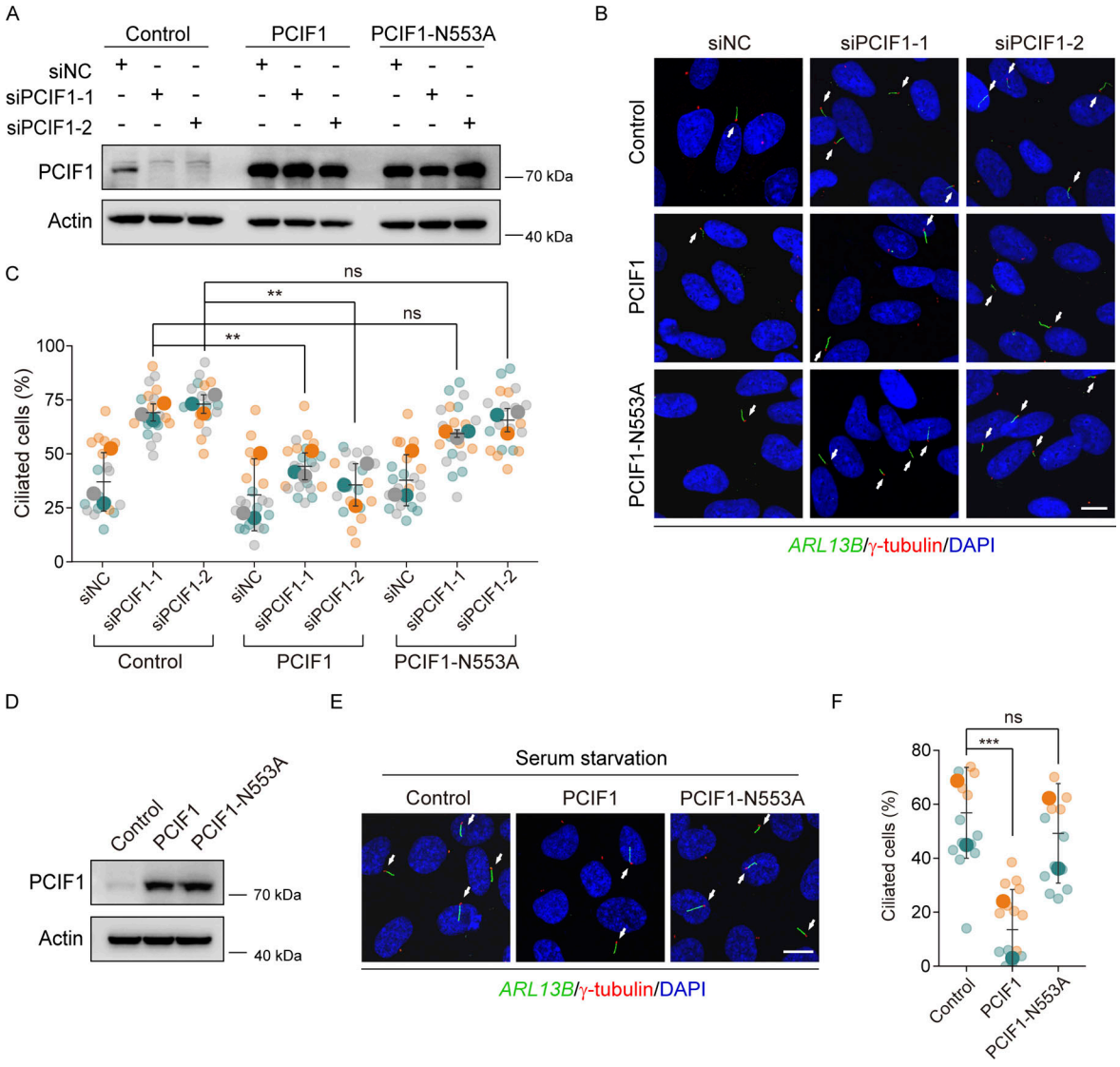

Figure 2. **PCIF1 inhibits ciliogenesis in an m^{6}Am-dependent manner. (A–C)** RPE-1 cells treated with the indicated siRNAs for 24 h were transfected with control, PCIF1, or PCIF1-N553A plasmid for another 36 h under normal culture conditions, and then subjected to Western analysis or immunofluorescence. **(D–F)** RPE-1 cells transfected with the indicated plasmids for 48 h were treated with serum starvation for another 24 h and then applied for Western analysis or immunofluorescence. Western blotting analysis of PCIF1 protein (A and D). Actin is the internal control. Immunofluorescence images of RPE-1 cells with anti-ARL13B (green) and γ-tubulin (red) antibodies (B and E). DNA was stained with DAPI (blue). Cilia were indicated by white arrows. Scale bar, 10 µm. Quantitative analysis of the ciliation percentage is presented using SuperPlots (C and F). Each color within the SuperPlots signifies an independent biological replicate. Smaller symbols denote the ciliation percentage under each field of view, while larger symbols represent the mean value for each replicate. All error bars represent means ± SD. Student's *t* test, **P < 0.01, ***P < 0.001, ns, not significant. Source data are available for this figure: SourceData F2.

whether PCIF1's impact on ciliation is associated with cell cycle regulation, we initially examined the consequences of PCIF1 deficiency on cell cycle progression in RPE-1 cells. Flow cytometry (FACS) analysis revealed that PCIF1 depletion increased the percentage of cells in the G0/G1 phase, indicative of cell cycle arrest (Fig. 6, A and B). Immunoblotting analyses unveiled reduced levels of cyclin A in PCIF1-depleted cells, suggesting a decrease in cells at the S or G2/M phase (Fig. 6 C). EdU-labeling experiments further demonstrated a decrease in the number of proliferating cells upon PCIF1 depletion (Fig. 6, D and E). These findings collectively indicate that PCIF1 depletion induces cell cycle arrest specifically at the G0/G1 phase.

Considering that IFT20, a crucial intraflagellar transport protein, is essential for cilia formation but has no substantial effect on cell cycle progression (Inaba et al., 2016; Zhang et al., 2021a, 2021b), we depleted IFT20 to impede cilia growth in PCIF1-depleted, aiming to discern whether the observed cell cycle arrest induced by PCIF1 depletion is mediated by enhanced ciliation. The data demonstrated a significant reduction in the enhanced ciliation in PCIF1-depleted cells upon IFT20 depletion (Fig. 6, F and G). Moreover, FACS profiles, immunoblotting, and EdU incorporation experiments revealed that the elimination of cilia induced by IFT20 depletion effectively reversed the G0/G1 arrest in PCIF1-depleted cells (Fig. 6), suggesting that PCIF1

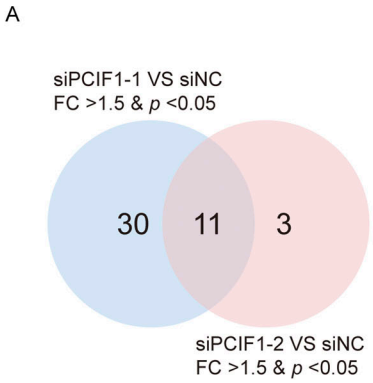

B

11 overlapping proteins from siPCIF1-1 and siPCIF1-2

Proteins	Fold changes	p value
OSBPL5	2.313	2.96E-04
INTS10	2.164	0.0405
OGFR	2.066	7.69E-05
BICD2	1.877	1.59E-05
SETD7	1.79	3.88E-05
DCBLD2	1.702	2.99E-05
CACNG6	1.632	2.08E-05
SEMA7A	1.586	3.32E-06
POMGNT1	1.567	0.019
WBP4	1.562	0.004
IFT27	1.549	1.56E-04

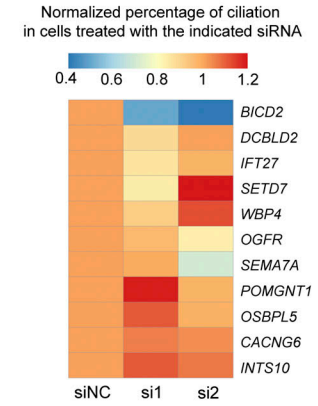

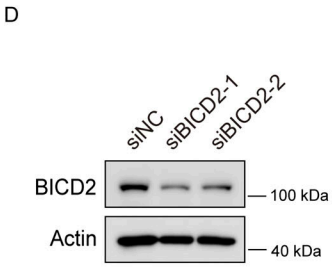

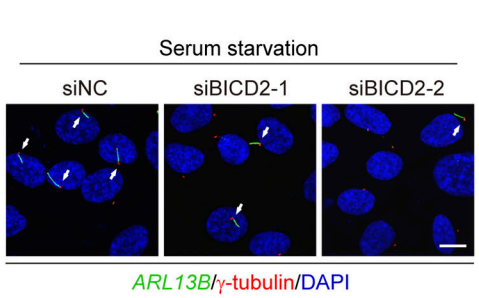

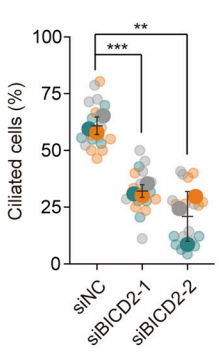

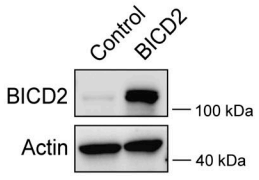

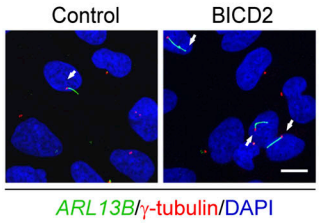

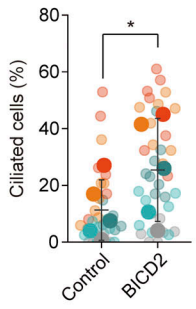

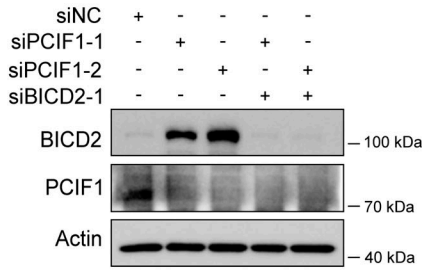

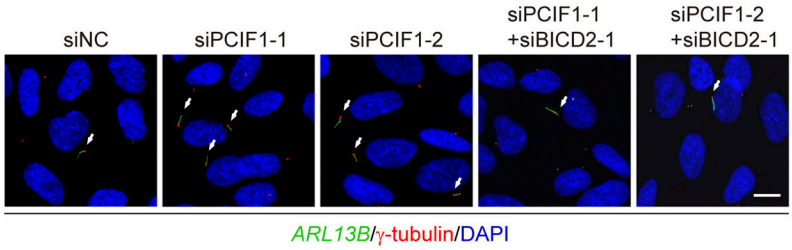

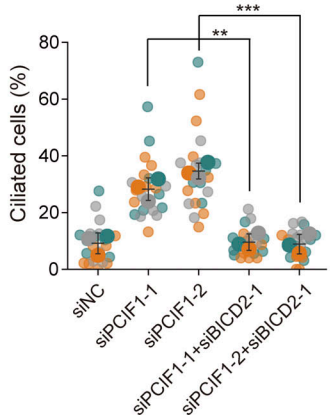

Figure 3. **PCIF1 suppresses ciliogenesis through BICD2. (A and B)** RPE-1 cells treated with the indicated siRNAs for 48 h were subjected to the tandem mass tag quantitative proteomics analysis. Venn diagram shows the overlapping upregulated proteins in RPE-1 cells treated with PCIF1 siRNAs (A). The overlapping upregulated proteins ranked by fold change are listed (B). **(C)** The heatmap of the normalized ratio of ciliated cells transfected with the indicated siRNAs targeting 11 overlapping upregulated proteins from TMT proteomics analysis. The normalized ratio of ciliated cells represents the quotient of the ciliated rate induced by siRNA relative to the ciliated rate induced by siNC. **(D–F)** RPE-1 cells transfected with control or *BICD2* siRNAs for 48 h were treated with serum starvation for another 24 h, and then subjected to western analysis or immunofluorescence. **(G–I)** RPE-1 cells were treated with control or BICD2 plasmid for 48 h under normal culture conditions, and then applied for Western blotting or immunofluorescence analysis. **(J–L)** RPE-1 cells were treated with

the indicated siRNAs for 48 h under normal culture conditions, and then applied for Western blotting or immunofluorescence analysis. Western blotting analysis of BICD2 and PCIF1 protein (D, G, and J). Actin is the internal control. Immunofluorescence images of RPE-1 cells with anti-ARL13B (green) and γ-tubulin (red) antibodies (E, H, and K). DNA was stained with DAPI (blue). Cilia were indicated by white arrows. Scale bar, 10 µm. The quantification analysis of ciliation percentages is presented in SuperPlots (F, I, and L). Each color in SuperPlots signifies an independent biological replicate. Smaller symbols indicate the ciliation percentage under each field of view, while larger symbols represent the mean for each replicate. All error bars represent means ± SD. Student's *t* test, *P < 0.05, **P < 0.01, ***P < 0.001. Source data are available for this figure: SourceData F3.

depletion causes cell cycle arrest at G0/G1 in a cilia-dependent manner.

Discussion

Our study shows the biological significance of PCIF1-mediated regulation of *BICD2* mRNA in mammalian cell ciliogenesis. PCIF1 adds m^{6}Am to *BICD2* mRNA, leading to reduced mRNA stability and translation, which suppresses BICD2 protein expression to inhibit ciliogenesis in mammalian cells (Fig. 7). These findings contribute valuable insights into the impact of RNA epigenetics on ciliogenesis, advancing our understanding of this complex biological process.

Previous studies suggest that PCIF1 regulates the accumulation of the homeodomain transcription factor PDX1, influencing the expression of insulin and other genes crucial for maintaining β cell mass and function in adult mice (Claiborn et al., 2010). Additionally, Pandey et al. (2020) demonstrated that *Pcif1* mutant mice exhibited reduced body weight without affecting viability and fertility (Pandey et al., 2020). Here, we found that PCIF1 negatively regulates ciliogenesis, and given the reported roles of primary cilia in controlling mammalian energy homeostasis and body weight (Vaisse et al., 2017), it is intriguing to explore whether PCIF1's contribution to ciliation plays a role in these physiological events.

The roles of m^{6}Am modifications in regulating mRNA transcription or translation remain unclear and context dependent. Suzuki's group reported that m^{6}Am promotes the translation of capped mRNAs in an eIF4E-independent manner without

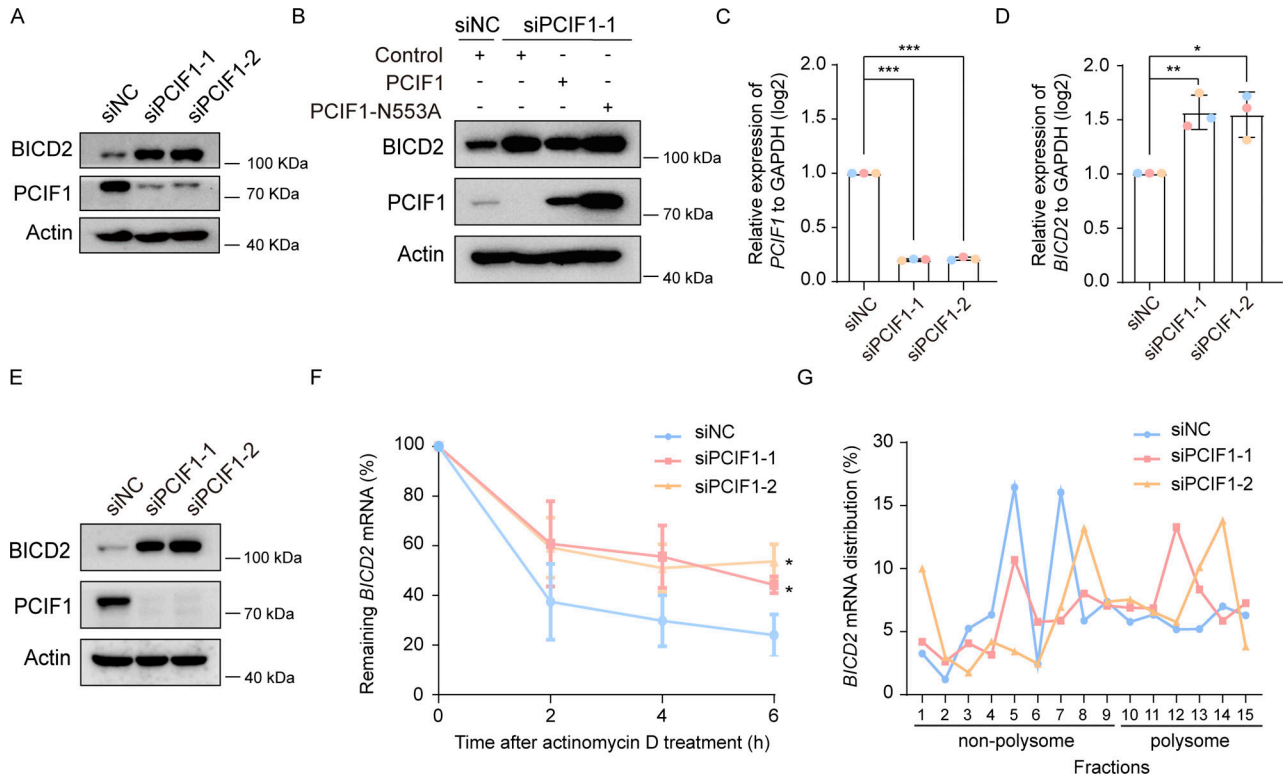

Figure 4. **PCIF1 knockdown promotes the stability and translation of *BICD2* mRNA. (A)** Western blotting analysis of BICD2 and PCIF1 protein of RPE-1 cells transfected with the indicated siRNAs for 48 h under normal culture conditions. Actin is the internal control. **(B)** Western blotting of BICD2 and PCIF1 proteins of RPE-1 cells treated with the indicated siRNAs for 24 h and transfected with the indicated plasmids for another 36 h under normal culture conditions. Actin is the internal control. **(C and D)** RT-qPCR (real-time quantitative PCR) analysis of *PCIF1* and *BICD2* mRNA of PCIF1 depleted RPE-1 cells. *GAPDH* is the internal control. **(E)** Western blot analysis of BICD2 and PCIF1 protein of RPE-1 cells transfected with the indicated siRNAs for 48 h under normal culture conditions. Actin is the internal control. **(F)** RT-qPCR of *BICD2* mRNA in PCIF1-depleted cells and control cells treated with actinomycin D (5 µg/ml). **(G)** Polysome profile of *BICD2* mRNA in cells transfected with the indicated siRNA after sucrose gradient centrifugation. Data are presented as the means ± SD from at least three independent experiments (C, D, and F). Student's *t* test, *P < 0.05, **P < 0.01, ***P < 0.001. Source data are available for this figure: SourceData F4.

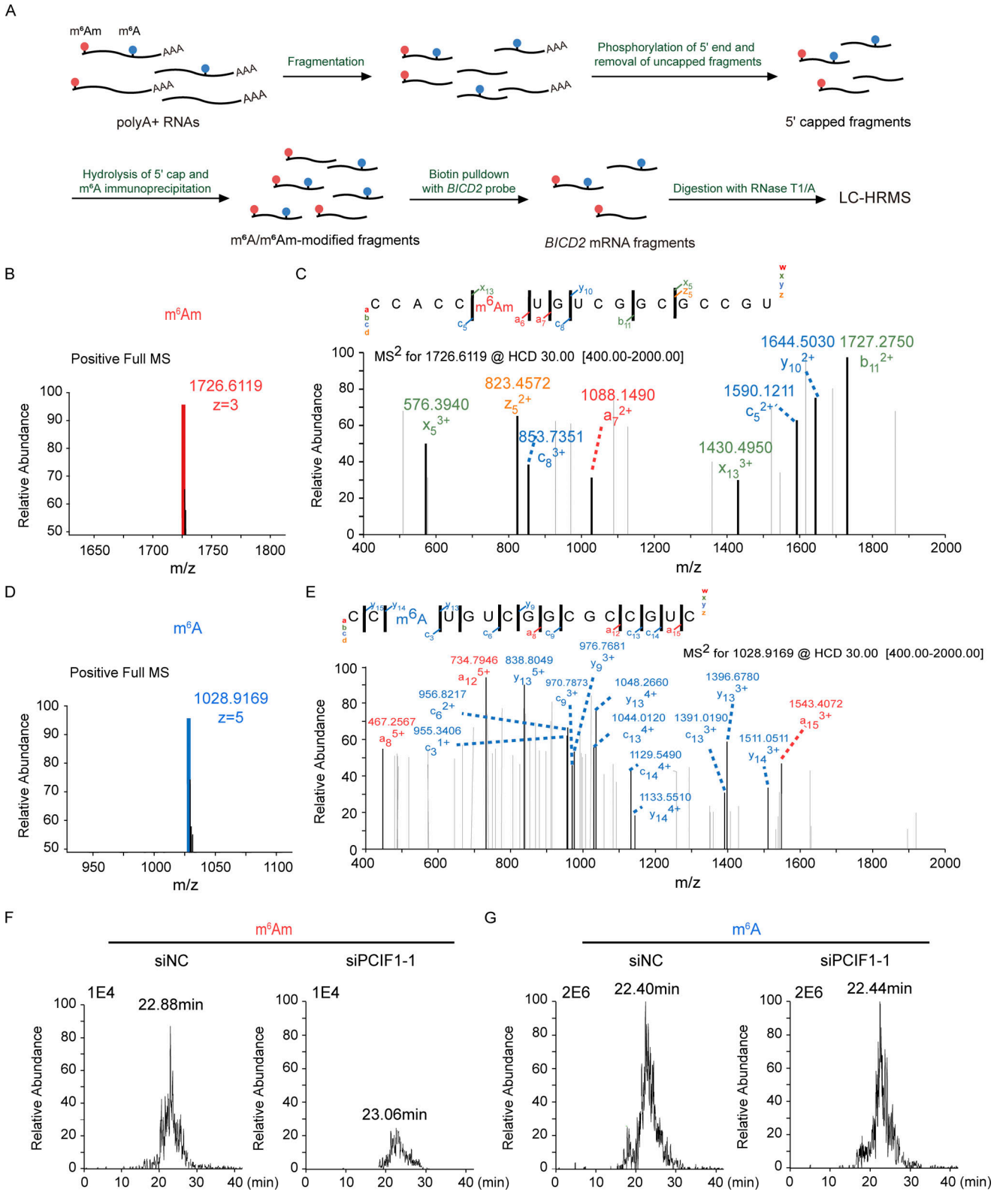

Figure 5. **Detection of the m^{6}Am site on *BICD2* mRNA. (A)** The scheme of the single-based resolution m^{6}Am fragments detection strategy by using liquid chromatography-high resolution mass spectrometry (LC-HRMS). **(B–E)** The primary and secondary MS results of the targeted fragment in BICD2 showing both m^{6}Am or m^{6}A sites detected in the second "A" of this fragment. **(F and G)** The total ion current (TIC) of the fragment containing m^{6}Am or m^{6}A modification with PCIF1 knockdown.

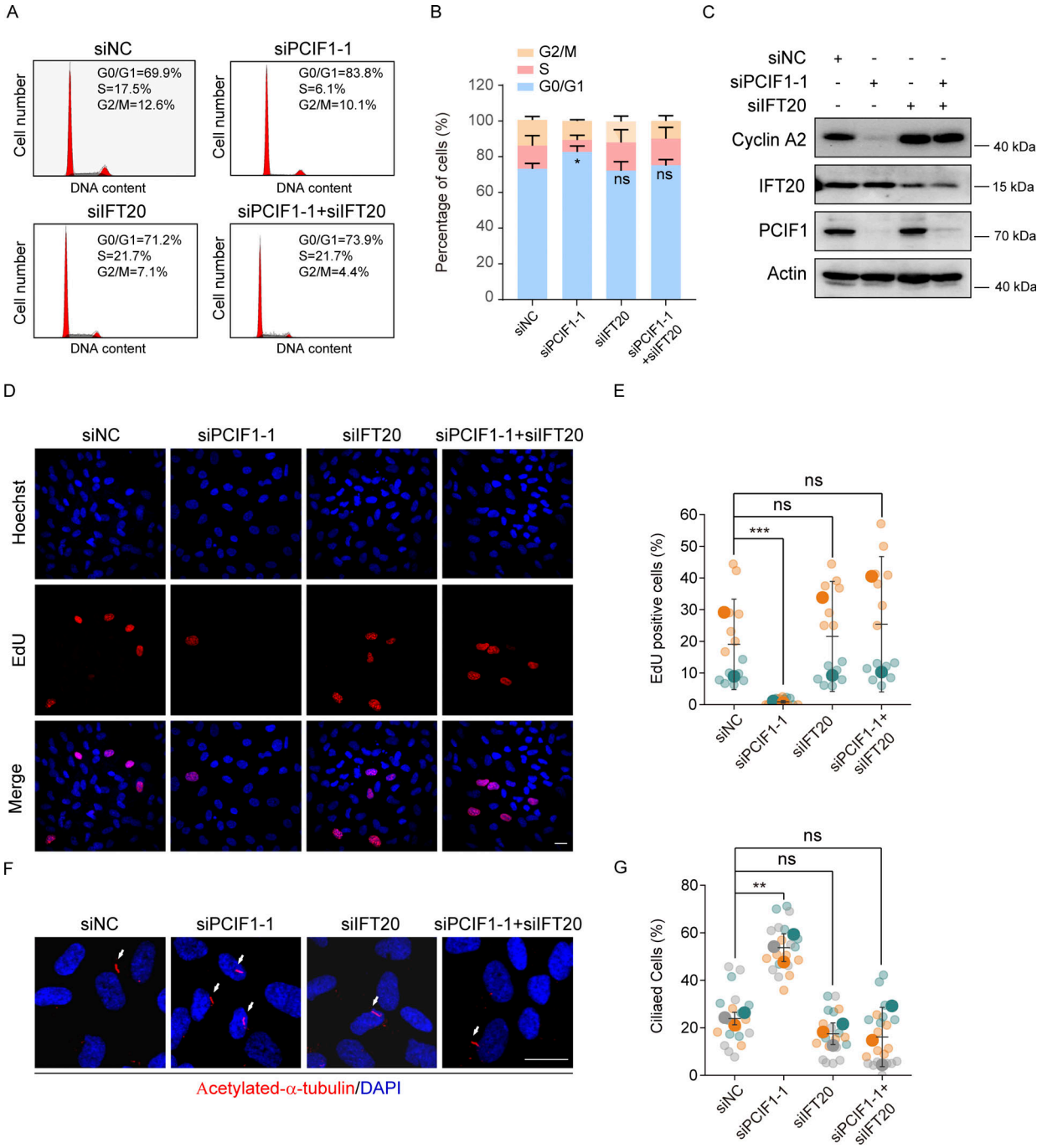

Figure 6. **PCIF1 deficiency induces a cilia-dependent cell cycle arrest.** RPE-1 cells cultured in normal conditions were treated with the indicated siRNAs for 48 h and then processed to the following analyses. **(A)** Graphical representations of the cell cycle distribution. **(B)** The percentages of cell populations in G0/G1, S, and G2/M phases. **(C)** Western blotting analysis of the Cyclin A2, IFT20, and PCIF1. Actin served as a loading control. **(D)** Immunofluorescence images of RPE-1 cells stained with EdU (red) and DNA (blue). Scale bar, 30 μm. **(E)** The percentages of EdU-positive cells were quantified. **(F)** Immunofluorescence images of RPE-1 cells with anti-ARL13B (green) and γ-tubulin (red) antibodies. DNA was stained with DAPI (blue). Cilia were indicated by white arrows. Scale bar, 10 μm. **(G)** Quantification analysis of the percentage of ciliated cells. Each color in SuperPlots represents an independent biological replicate. Smaller symbols are the percentages of EdU-positive cells (E) or the percentage of ciliated cells under each field of view (G), and larger symbols are the mean of each replicate. All error bars represent means ± SD. Student's *t* test, *P < 0.05, **P < 0.01, ***P < 0.001, ns, not significant. Source data are available for this figure: SourceData F6.

affecting transcriptome alteration (Akichika et al., 2019). Conversely, Sendinc et al. found that m^{6}Am negatively impacted cap-dependent translation of methylated mRNAs in PCIF1 knockout MEL624 cells (Sendinc et al., 2019). Other studies propose that m^{6}Am might modulate mRNA stability. Hirose et al. reported that PCIF1 negatively regulates transcription, although the mechanism remains unclear (Hirose et al., 2008). Additionally, it is found that m^{6}Am modifications at the beginning of mRNAs increase stability, with an average increase in the half-life of around 2.5 h compared with non-methylated

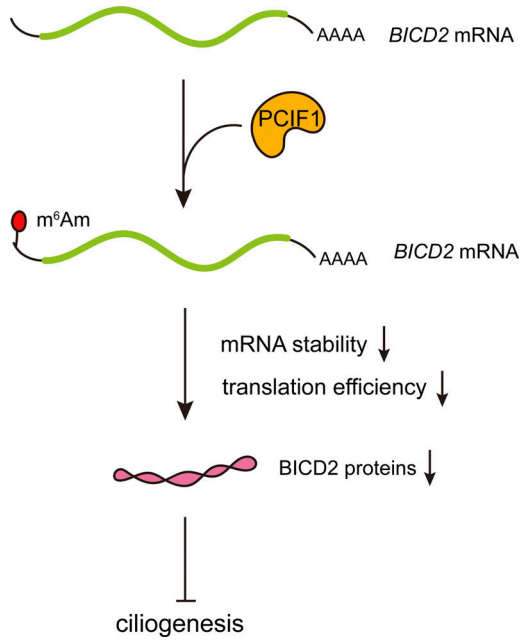

Figure 7. **Working model of PCIF1-mediated m^{6}Am modification on *BICD2* mRNA to regulate ciliogenesis.** PCIF1 modifies m^{6}Am on *BICD2* mRNA, leading to reduced mRNA stability and translation, which suppresses BICD2 protein expression to inhibit ciliogenesis in mammalian cells.

bases (Mauer et al., 2017). Boulias et al. also demonstrated that depleting PCIF1 minimally affects mRNA translation but leads to reduced stability of a subset of m^{6}Am-annotated mRNAs in HEK293T cells (Boulias et al., 2019). Moreover, the loss of cap-specific m^{6}Am RNA methylation in mice resulted in transcript destabilization (Pandey et al., 2020). These contrasting findings necessitate further investigations to unravel the context-dependent roles of m^{6}Am and PCIF1 in mRNA regulation.

Dynein-2, also known as IFT dynein, is a motor protein complex essential for the structure and function of cilia (Vuolo et al., 2018). Since BICD2 is not a component in the dynein-2 complex (Asante et al., 2014), it may not directly enter cilia or regulate the retrograde IFT. However, BICD2 is an adaptor protein that facilitates the interaction between cytoplasmic dynein-1 and its cargo (Hoogenraad et al., 2001). The altered levels of BICD2 due to PCIF1 dysfunction will impact various cellular processes mediated by dynein-1, including membrane traffic, organelle dynamics, and centrosome and nuclear positioning (Grigoriev et al., 2007; Matanis et al., 2002; Short et al., 2002; Splinter et al., 2012). Though dynein-1 is not directly involved in the movement of cilia, it influences ciliogenesis by facilitating the intracellular transport of key components required for cilia assembly and maintenance (Palmer et al., 2011; Roberts et al., 2013). Consequently, the aberrance production of BICD2 and resultant dynein-1 dysfunction may affect ciliogenesis. Additionally, BICD2 has been identified as a component of centriolar satellite proteins (Quarantotti et al., 2019), which play a crucial role in basal body maturation and function (Tollenaere et al., 2015). This suggests that the localization of BICD2 in centriolar satellites may also contribute to the regulation of ciliation. Future investigations are clearly needed to decipher the molecular mechanisms governing the regulation of ciliogenesis orchestrated by BICD2.

Materials and methods

Cell culture and transfection

Human telomerase reverse transcriptase–immortalized retinal pigment epithelial cells (hTERT RPE-1) were obtained from the American Type Culture Collection (ATCC) and cultured in DMEM/F12 medium (Corning) supplemented with 10% fetal bovine serum (FBS; ExCell Bio) at 37°C in a 5% CO_2 incubator. Serum starvation involved culturing cells in DMEM/F12 without FBS at 37°C in a 5% CO_2 incubator. For transfections, Lipofectamine iMAX (Invitrogen) or Lipofectamine 3000 (Invitrogen) was used as per the manufacturer's instructions. Transfection efficiencies were assessed via Western blot or qRT-PCR analysis. The siRNA sequences are provided in Table S4.

Plasmids

The full-length human *PCIF1* gene was amplified from cDNAs and subsequently cloned into the pCS2+ vector. The *PCIF1-N553A* mutation was generated by PCR amplified from wild-type *PCIF1* plasmid.

RNA extraction and quantitative real-time PCR

Total RNA was extracted using the TRIzol reagent (Ambion), and cDNA was synthesized using the HiScript II first strand cDNA Synthesis kit (Vazyme). Quantitative real-time PCR (qRT-PCR) was performed on a Roche 480II-384 System using the HiScript Q RT SuperMix (Vazyme). Primer sequences are provided in Table S5.

Western blot

For Western blot assays, cells were lysed with TBSN buffer (20 mM Tris-HCl, pH 8.0, 150 mM NaCl, 0.5% NP-40, 5 mM EGTA, 1.5 mM EDTA, 0.5 mM Na_3VO_4, and 20 mM p-nitrophenyl phosphate) and supplemented with protease inhibitor cocktails (04693132001; Roche). The cell lysates were then subjected to SDS-PAGE, and the proteins were transferred onto polyvinylidene fluoride membranes (Millipore). The membranes were blocked with 5% non-fat milk in PBST (PBS containing 0.1% Tween-20) for 1 h at room temperature and then incubated overnight at 4°C with the respective primary antibodies. After washing three times with PBST for 5 min each, the membranes were incubated with HRP-conjugated secondary antibodies for 1 h at room temperature, followed by three additional washes with PBST for 5 min each. Protein bands were visualized using the ChemiDoc Touch Imaging System (Bio-Rad).

Immunofluorescence staining

Immunofluorescence assays were carried out as described previously (Liu et al., 2021). Cells cultured on coverslips were fixed with 100% methanol at −20°C for 10 min and then blocked with 5% BSA in $PBST_X$ (PBS containing 0.1% Triton X-100) for 1 h at room temperature. Subsequently, the cells were incubated overnight with the respective primary antibodies diluted in the

blocking buffer at 4°C. After three washes with $PBST_X$ for 5 min each, the cells were incubated with species-specific Alexa 488/555 fluorochrome-conjugated secondary antibodies diluted in a blocking buffer for 1 h at room temperature in a dark room. Following three additional washes with $PBST_X$ for 5 min each, the nuclei were stained with DAPI (564907; BD Biosciences). Confocal images were randomly acquired using an OLYMPUS FV3000 OSR laser scanning confocal microscope at room temperature using a 60×/1.42 oil objective (Fig. 6, D and F; Fig. S1, B, E, H, K, and N; and Fig. S2, B, E, H, K, and N) or a 63×/1.40 oil objective on Zeiss LSM 880 microscope (Fig. 1, B, F, and I; and Fig. 2, B and E; Fig. 3, D, G, and J). The acquisition settings were consistent for both the experimental and control groups within the same experiment. For the quantification process, we consistently selected seven to nine random fields within each experimental group to count both the number of cells (based on DAPI staining) and the cilia signal. Subsequently, we utilized Photoshop software to quantify the number of cells and cilia. Specifically, cilia length was measured from the base to the tip of the cilia.

Tandem mass tag quantitative MS and data analysis

RPE-1 cells were transfected with control or PCIF1 siRNAs in a 10% serum-containing DMEM/F12 medium for 48 h. Following transfection, cells were collected and underwent TMT quantitative proteomic analysis by Jingjie PTM BIO. Peptides were processed using NSI and analyzed by MS/MS on a Q ExactiveTM Plus instrument coupled with UPLC. Maxquant search engine (v.1.5.2.8) was used for data analysis, with spectra interrogated against the human Uniprot database and a reverse decoy database. Quantitative analysis employed TMT 10-plex, with both protein and PSM identification filtered rigorously at a 1% FDR threshold.

5,856 proteins were identified in total. To facilitate data sharing and accessibility, the raw proteomics data and search results were deposited in the PRIDE archive, accessible through the ProteomeXchange accession number PXD044338.

To calculate the fold change between PCIF1 si1/2 and NC group, the formula is shown as follows: *FC* denotes the fold change of the protein. *R* denotes the relative quantitative value of the protein, *i* denotes the sample, and *k* denotes the protein.

$$FC_{si/NC,k} = \mathrm{Mean}(R_{ik}, i \in si) / \mathrm{Mean}(R_{ik}, i \in NC)$$

The relative quantitative value of proteins was used for differential expressed proteins analysis. Student's *t* test was performed to calculate the statistical significance of difference between groups. Proteins with P value <0.05 and Fold Change >1.5 was regarded as significantly upregulated proteins, while the protein with P value <0.05 and Fold Change <0.667 were regarded as significantly downregulated proteins.

Single-base resolution m^{6}Am site detection

The m^{6}A RNA immunoprecipitation (MeRIP) was conducted using the Magna MeRIP m^{6}A kit (17-10499; Millipore) following the manufacturer's instructions. Subsequently, the resulting complementary DNA fragments were utilized as probes to enrich targeted mRNAs containing m^{6}Am sites. The length of the DNA probe was 25 nt and it had biotin at the terminal. The DNA probe had a length of 25 nucleotides with biotin at the terminal, and the specific sequences for targeting *BICD2* were 5′-AGGGCG GCGGCGGCGGCGGCAGCGG-3′ and 5′-TCGGCCACCATGTCG GCGCCGTCGG-3′. The hybridization process lasted for 3 h, maintaining a probe-to-mRNA ratio of 1.25:1 (mol/ml). To obtain ∼25 nucleotide fragments, the targeted digestion of mRNA was performed using the RNase T1/A mix kit (EN0551; Thermo Fisher Scientific), following the instructions provided with the kit. The digestion method was according to the instructions of the RNase mix kit. Finally, the digested mRNA fragments were eluted with 50% formamide and analyzed using Nano-liquid chromatography-high resolution mass spectrometry (LC-HRMS) on a Thermo QE HF instrument. The MS/MS data was processed using Thermo Xcalibur 2.7 software, and RNA fragments with a signal-to-noise ratio (SNR) >10 were considered valid peaks. The sequencing analysis of these RNA fragments was performed using an online software tool (https://Ariadne.riken.jp/html/search.html).

mRNA decay assay

The mRNA decay assay was conducted following the protocol described in Kuang et al. (2022). After transfection with control or PCIF1 siRNAs for 48 h, RPE-1 cells were treated with 5 µg/ml actinomycin D (HY-17559; MedChemExpress) to inhibit global mRNA transcription. Subsequently, cells were harvested at the designated time points and total RNAs were extracted for reverse transcription. The expression levels of *BICD2* mRNA, following transcription inhibition, were analyzed using qRT-PCR.

Polysome fractionation

Polysome fractionation was carried out following the protocol described in Gandin et al. (2014). Briefly, control or PCIF1-depleted RPE-1 cells (three 150-mm culture dishes) were treated with cycloheximide (HY-12320; MedChemExpress) at a final concentration of 100 µg/ml in growth media for 5 min at 37°C and 5% CO_2. The cells were then washed twice with 10 ml of ice-cold 1× PBS containing 100 µg/ml cycloheximide. After that, the cells were collected and resuspended in 425 µl of hypotonic buffer (5 mM Tris-HCl [pH 7.5], 2.5 mM $MgCl_2$, 1.5 mM KCl, and 1× protease inhibitor cocktail [EDTA-free]). To the cell suspension, 5 µl of 10 mg/ml cycloheximide, 1 µl of 1 M DTT, and 100 U of RNAse inhibitor were added. The mixture was vortexed for 5 s, followed by the addition of 25 µl of 10% Triton X-100 (final concentration 0.5%) and 25 µl of 10% sodium deoxycholate (final concentration 0.5%). The mixture was vortexed again for 5 s. After centrifugation of the lysates at 16,000 *g* for 7 min at 4°C, the supernatant was transferred, and the absorbance was measured at 260 nm to determine the RNA concentration. Subsequently, the supernatant was loaded onto a 5–50% sucrose gradient and centrifuged at 36,000 rpm for 2 h at 4°C using an SW41Ti rotor (Beckman). The gradients were fractionated and absorbance at 254 nm was monitored using a fraction collector (Biocomp). Polysome-associated and cytosolic RNAs from each fraction were extracted using TRIzol protocol according to the manufacturer's instructions, and their levels were monitored by qRT-PCR.

Flow cytometry analysis

For flow cytometry analysis, RPE-1 cells were harvested and washed once with ice-cold 1× PBS. Subsequently, the cells were resuspended in ice-cold 1× PBS and fixed by incubating in ice-cold 95% ethanol at −20°C overnight. To stain the DNA, the cells were treated with 100 µg/ml propidium iodide and 50 µg/ml RNase A for 30 min at 37°C. Finally, the samples were analyzed using an FC 500 MCL Flow Cytometer (Beckman Coulter). We conducted three biological replicates for the flow cytometry analysis, involving the transfection of cells with siRNAs and subsequent flow cytometry analysis on separate occasions. Each occasion utilized distinct batches of cell samples.

EdU assay

Before and during Edu experiments, the cells were cultured in normal conditions (DMEM/F12 medium with 10% serum). RPE-1 cells were incubated with 50 µM EdU (5-Ethynyl-2′-deoxyuridine) diluted in DMEM/F12 medium with 10% serum for 2 h. After incubation, the cells were fixed in 4% PFA for 30 min at room temperature. EdU staining was performed using the Cell-Light EdU Apollo567 In Vitro Kit (C10310-1; Ribobio) following the manufacturer's instructions.

Antibodies

Antibodies used in this study for Western blot included rabbit anti-PCIF1 (1:1,000, ab300487; Abcam), rabbit anti- BICD2 (1:1,000, NBP1-81488; Novus Biologicals), rabbit anti- cyclin A2 (1:1,000, 18202-1-AP; Proteintech), rabbit anti- IFT20 (1:500, 13615-1-AP; Proteintech), mouse anti-ACTIN (1:2,000, 66009-1-Ig; Proteintech), HRP Goat anti-Mouse IgG (1:5,000, AS003; Abclonal), and HRP Goat anti-Rabbit IgG (1:5,000, AS014; Abclonal). Antibodies used in this study for immunofluorescence included rabbit anti-ARL13B (1:200, 17711-1-AP; Proteintech), mouse anti-γ-tubulin (1:1,000, T6557; Sigma-Aldrich), mouse anti-acetylated-α-tubulin (1:1,000, T7451; Sigma-Aldrich), Alexa Fluor 488-conjugated anti-rabbit IgG (1:200, A21206; Invitrogen), and Alexa Fluor 555-conjugated anti-mouse IgG (1:200, A31570; Invitrogene).

Statistical analysis

The means and standard deviations (SD) were calculated and are shown in the graphs. Student's *t* test was applied to assess statistical significance. SuperPlots (Lord et al., 2020) and heatmaps were produced in R programming language (version 4.2.3).

Language editing

ChatGPT3.5 was employed to refine the language of the manuscript using the command "Below is an academic paper. Polish the writing to meet the academic style, improve spelling, grammar, clarity, and overall readability."

Online supplemental material

Fig. S1 shows the effect of *OSBPL5*, *NTS10*, *OGFR*, *SETD7*, and DCBLD2 knockdown on ciliation. Fig. S2 shows the effect of CACNG6, SEMA7A, POMGNT1, WBP4, and IFT27 genes knockdown on ciliation. Table S1 shows analysis of TMT proteomics. Table S2 shows significant hit proteins for siPCIF1-1 versus its control. Table S3 shows significant hit proteins for siPCIF1-2 versus its control. Table S4 shows sequences of siRNAs. Table S5 shows sequences of primers.

Data availability

Data is accessible in the main text or supplementary materials. For additional details, resource inquiries, and reagent requests, please contact the lead, Tianhua Zhou (tzhou@zju.edu.cn).

Acknowledgments

We are grateful to Shuangshuang Liu, Guifeng Xiao, Junli Xuan, and Wei Yin for their help in the confocal laser scanning microscope. We thank Wanling Zheng (Zhejiang University) for helping with the polysome profiling assay.

This work was supported by the National Natural Science Foundation of China (U21A20197 and 32270723) and the National Key Research and Development Program of China (2019YFA0802202).

Author contributions: S. Xie and T. Zhou conceived the work. S. Xie and W. Kuang designed and performed most of the experiments. M. Guo conducted the experiments on m^{6}Am site analysis. F. Yang performed the bioinformatics and statistical analysis. H. Jin and X. Chen performed part of the experiments about BICD2. C. Huo and Z. Xu carried out the polysome profiling assay. X. Chen and L. Yi performed cell cycle analysis. S. Xie and T. Zhou wrote the manuscript. Q. Shu, J. Mao, W. Liu, and A. Lin edited the manuscript.

Disclosures: The authors declare no competing interests exist.

Submitted: 7 July 2023
Revised: 7 January 2024
Accepted: 29 February 2024

References

Akichika, S., S. Hirano, Y. Shichino, T. Suzuki, H. Nishimasu, R. Ishitani, A. Sugita, Y. Hirose, S. Iwasaki, O. Nureki, and T. Suzuki. 2019. Cap-specific terminal N ^{6}-methylation of RNA by an RNA polymerase II-associated methyltransferase. *Science*. 363:eaav0080. https://doi.org/10.1126/science.aav0080

Anvarian, Z., K. Mykytyn, S. Mukhopadhyay, L.B. Pedersen, and S.T. Christensen. 2019. Cellular signalling by primary cilia in development, organ function and disease. *Nat. Rev. Nephrol.* 15:199–219. https://doi.org/10.1038/s41581-019-0116-9

Asante, D., N.L. Stevenson, and D.J. Stephens. 2014. Subunit composition of the human cytoplasmic dynein-2 complex. *J. Cell Sci.* 127:4774–4787. https://doi.org/10.1242/jcs.159038

Boulias, K., D. Toczydłowska-Socha, B.R. Hawley, N. Liberman, K. Takashima, S. Zaccara, T. Guez, J.J. Vasseur, F. Debart, L. Aravind, et al. 2019. Identification of the m^{6}Am methyltransferase PCIF1 reveals the location and functions of m^{6}Am in the transcriptome. *Mol. Cell*. 75:631–643.e8. https://doi.org/10.1016/j.molcel.2019.06.006

Claiborn, K.C., M.M. Sachdeva, C.E. Cannon, D.N. Groff, J.D. Singer, and D.A. Stoffers. 2010. Pcif1 modulates Pdx1 protein stability and pancreatic β cell function and survival in mice. *J. Clin. Invest.* 120:3713–3721. https://doi.org/10.1172/JCI40440

Cowling, V.H. 2019. CAPAM: The mRNA cap adenosine N6-methyltransferase. *Trends Biochem. Sci.* 44:183–185. https://doi.org/10.1016/j.tibs.2019.01.002

Gandin, V., K. Sikström, T. Alain, M. Morita, S. McLaughlan, O. Larsson, and I. Topisirovic. 2014. Polysome fractionation and analysis of mammalian

translatomes on a genome-wide scale. *J. Vis. Exp.* 87:51455. https://doi.org/10.3791/51455
Grigoriev, I., D. Splinter, N. Keijzer, P.S. Wulf, J. Demmers, T. Ohtsuka, M. Modesti, I.V. Maly, F. Grosveld, C.C. Hoogenraad, and A. Akhmanova. 2007. Rab6 regulates transport and targeting of exocytotic carriers. *Dev. Cell.* 13:305–314. https://doi.org/10.1016/j.devcel.2007.06.010
Hirose, Y., Y. Iwamoto, K. Sakuraba, I. Yunokuchi, F. Harada, and Y. Ohkuma. 2008. Human phosphorylated CTD-interacting protein, PCIF1, negatively modulates gene expression by RNA polymerase II. *Biochem. Biophys. Res. Commun.* 369:449–455. https://doi.org/10.1016/j.bbrc
Hoogenraad, C.C., A. Akhmanova, S.A. Howell, B.R. Dortland, C.I. De Zeeuw, R. Willemsen, P. Visser, F. Grosveld, and N. Galjart. 2001. Mammalian Golgi-associated Bicaudal-D2 functions in the dynein-dynactin pathway by interacting with these complexes. *EMBO J.* 20:4041–4054. https://doi.org/10.1093/emboj/20.15.4041
Hoogenraad, C.C., P. Wulf, N. Schiefermeier, T. Stepanova, N. Galjart, J.V. Small, F. Grosveld, C.I. de Zeeuw, and A. Akhmanova. 2003. Bicaudal D induces selective dynein-mediated microtubule minus end-directed transport. *EMBO J.* 22:6004–6015. https://doi.org/10.1093/emboj/cdg592
Huynh, W., and R.D. Vale. 2017. Disease-associated mutations in human BICD2 hyperactivate motility of dynein-dynactin. *J. Cell Biol.* 216:3051–3060. https://doi.org/10.1083/jcb.201703201
Inaba, H., H. Goto, K. Kasahara, K. Kumamoto, S. Yonemura, A. Inoko, S. Yamano, H. Wanibuchi, D. He, N. Goshima, et al. 2016. Ndel1 suppresses ciliogenesis in proliferating cells by regulating the trichoplein-Aurora A pathway. *J. Cell Biol.* 212:409–423. https://doi.org/10.1083/jcb.201507046
Kasahara, K., and M. Inagaki. 2021. Primary ciliary signaling: Links with the cell cycle. *Trends Cell Biol.* 31:954–964. https://doi.org/10.1016/j.tcb.2021.07.009
Keith, J.M., M.J. Ensinger, and B. Moss. 1978. HeLa cell RNA (2′-O-methyl-adenosine-N6-)-methyltransferase specific for the capped 5′-end of messenger RNA. *J. Biol. Chem.* 253:5033–5039. https://doi.org/10.1016/S0021-9258(17)34652-5
Kim, H., Y.S. Lee, S.M. Kim, S. Jang, H. Choi, J.W. Lee, T.D. Kim, and V.N. Kim. 2021. RNA demethylation by FTO stabilizes the FOXJ1 mRNA for proper motile ciliogenesis. *Dev. Cell.* 56:1118–1130.e6. https://doi.org/10.1016/j.devcel.2021.03.006
Kuang, W., H. Jin, F. Yang, X. Chen, J. Liu, T. Li, Y. Chang, M. Liu, Z. Xu, C. Huo, et al. 2022. ALKBH3-dependent m^1A demethylation of Aurora A mRNA inhibits ciliogenesis. *Cell Discov.* 8:25. https://doi.org/10.1038/s41421-022-00385-3
Liu, M., W. Zhang, M. Li, J. Feng, W. Kuang, X. Chen, F. Yang, Q. Sun, Z. Xu, J. Hua, et al. 2021. NudCL2 is an autophagy receptor that mediates selective autophagic degradation of CP110 at mother centrioles to promote ciliogenesis. *Cell Res.* 31:1199–1211. https://doi.org/10.1038/s41422-021-00560-3
Lord, S.J., K.B. Velle, R.D. Mullins, and L.K. Fritz-Laylin. 2020. SuperPlots: Communicating reproducibility and variability in cell biology. *J. Cell Biol.* 219:e202001064. https://doi.org/10.1083/jcb.202001064
Matanis, T., A. Akhmanova, P. Wulf, E. Del Nery, T. Weide, T. Stepanova, N. Galjart, F. Grosveld, B. Goud, C.I. De Zeeuw, et al. 2002. Bicaudal-D regulates COPI-independent Golgi-ER transport by recruiting the dynein-dynactin motor complex. *Nat. Cell Biol.* 4:986–992. https://doi.org/10.1038/ncb891
Mauer, J., X. Luo, A. Blanjoie, X. Jiao, A.V. Grozhik, D.P. Patil, B. Linder, B.F. Pickering, J.J. Vasseur, Q. Chen, et al. 2017. Reversible methylation of m^6A_m in the 5′ cap controls mRNA stability. *Nature.* 541:371–375. https://doi.org/10.1038/nature21022
Nachury, M.V., and D.U. Mick. 2019. Establishing and regulating the composition of cilia for signal transduction. *Nat. Rev. Mol. Cell Biol.* 20:389–405. https://doi.org/10.1038/s41580-019-0116-4
Palmer, K.J., L. MacCarthy-Morrogh, N. Smyllie, and D.J. Stephens. 2011. A role for Tctex-1 (DYNLT1) in controlling primary cilium length. *Eur. J. Cell Biol.* 90:865–871. https://doi.org/10.1016/j.ejcb.2011.05.003
Pandey, R.R., E. Delfino, D. Homolka, A. Roithova, K.M. Chen, L. Li, G. Franco, C.B. Vågbø, E. Taillebourg, M.O. Fauvarque, and R.S. Pillai. 2020. The mammalian cap-specific m^6Am RNA methyltransferase PCIF1 regulates transcript levels in mouse tissues. *Cell Rep.* 32:108038. https://doi.org/10.1016/j.celrep.2020.108038
Quarantotti, V., J.X. Chen, J. Tischer, C. Gonzalez Tejedo, E.K. Papachristou, C.S. D'Santos, J.V. Kilmartin, M.L. Miller, and F. Gergely. 2019. Centriolar satellites are acentriolar assemblies of centrosomal proteins. *EMBO J.* 38:e101082. https://doi.org/10.15252/embj.2018101082
Reck-Peterson, S.L., W.B. Redwine, R.D. Vale, and A.P. Carter. 2018. The cytoplasmic dynein transport machinery and its many cargoes. *Nat. Rev. Mol. Cell Biol.* 19:382–398. https://doi.org/10.1038/s41580-018-0004-3
Reiter, J.F., and M.R. Leroux. 2017. Genes and molecular pathways underpinning ciliopathies. *Nat. Rev. Mol. Cell Biol.* 18:533–547. https://doi.org/10.1038/nrm.2017.60
Roberts, A.J., T. Kon, P.J. Knight, K. Sutoh, and S.A. Burgess. 2013. Functions and mechanics of dynein motor proteins. *Nat. Rev. Mol. Cell Biol.* 14:713–726. https://doi.org/10.1038/nrm3667
Schlager, M.A., H.T. Hoang, L. Urnavicius, S.L. Bullock, and A.P. Carter. 2014. In vitro reconstitution of a highly processive recombinant human dynein complex. *EMBO J.* 33:1855–1868. https://doi.org/10.15252/embj.201488792
Sendinc, E., D. Valle-Garcia, A. Dhall, H. Chen, T. Henriques, J. Navarrete-Perea, W. Sheng, S.P. Gygi, K. Adelman, and Y. Shi. 2019. PCIF1 catalyzes m6Am mRNA methylation to regulate gene expression. *Mol. Cell.* 75:620–630.e9. https://doi.org/10.1016/j.molcel.2019.05.030
Short, B., C. Preisinger, J. Schaletzky, R. Kopajtich, and F.A. Barr. 2002. The Rab6 GTPase regulates recruitment of the dynactin complex to Golgi membranes. *Curr. Biol.* 12:1792–1795. https://doi.org/10.1016/S0960-9822(02)01221-6
Splinter, D., D.S. Razafsky, M.A. Schlager, A. Serra-Marques, I. Grigoriev, J. Demmers, N. Keijzer, K. Jiang, I. Poser, A.A. Hyman, et al. 2012. BICD2, dynactin, and LIS1 cooperate in regulating dynein recruitment to cellular structures. *Mol. Biol. Cell.* 23:4226–4241. https://doi.org/10.1091/mbc.e12-03-0210
Sun, H., M. Zhang, K. Li, D. Bai, and C. Yi. 2019. Cap-specific, terminal N^6-methylation by a mammalian m^6Am methyltransferase. *Cell Res.* 29:80–82. https://doi.org/10.1038/s41422-018-0117-4
Suter, B., L.M. Romberg, and R. Steward. 1989. Bicaudal-D, a Drosophila gene involved in developmental asymmetry: Localized transcript accumulation in ovaries and sequence similarity to myosin heavy chain tail domains. *Genes Dev.* 3:1957–1968. https://doi.org/10.1101/gad.3.12a.1957
Tartell, M.A., K. Boulias, G.B. Hoffmann, L.M. Bloyet, E.L. Greer, and S.P.J. Whelan. 2021. Methylation of viral mRNA cap structures by PCIF1 attenuates the antiviral activity of interferon-β. *Proc. Natl. Acad. Sci. USA.* 118:e2025769118. https://doi.org/10.1073/pnas.2025769118
Tollenaere, M.A., N. Mailand, and S. Bekker-Jensen. 2015. Centriolar satellites: Key mediators of centrosome functions. *Cell. Mol. Life Sci.* 72:11–23. https://doi.org/10.1007/s00018-014-1711-3
Vaisse, C., J.F. Reiter, and N.F. Berbari. 2017. Cilia and obesity. *Cold Spring Harb. Perspect. Biol.* 9:a028217. https://doi.org/10.1101/cshperspect.a028217
Vuolo, L., N.L. Stevenson, K.J. Heesom, and D.J. Stephens. 2018. Dynein-2 intermediate chains play crucial but distinct roles in primary cilia formation and function. *Elife.* 7:e39655. https://doi.org/10.7554/eLife.39655
Wang, L., L. Wu, Z. Zhu, Q. Zhang, W. Li, G.M. Gonzalez, Y. Wang, and T.M. Rana. 2023. Role of PCIF1-mediated 5′-cap N6-methyladeonsine mRNA methylation in colorectal cancer and anti-PD-1 immunotherapy. *EMBO J.* 42:e111673. https://doi.org/10.15252/embj.2022111673
Wei, C., A. Gershowitz, and B. Moss. 1975. N6, O2′-dimethyladenosine a novel methylated ribonucleoside next to the 5′ terminal of animal cell and virus mRNAs. *Nature.* 257:251–253. https://doi.org/10.1038/257251a0
Zhang, Q., Y. Kang, S. Wang, G.M. Gonzalez, W. Li, H. Hui, Y. Wang, and T.M. Rana. 2021a. HIV reprograms host m6Am RNA methylome by viral Vpr protein-mediated degradation of PCIF1. *Nat Commun.* 12:5543. https://doi.org/10.1038/s41467-021-25683-4
Zhang, Y.C., Y.F. Bai, J.F. Yuan, X.L. Shen, Y.L. Xu, X.X. Jian, S. Li, Z.Q. Song, H.B. Hu, P.Y. Li, et al. 2021b. CEP55 promotes cilia disassembly through stabilizing Aurora A kinase. *J Cell Biol.* 220:e202003149. https://doi.org/10.1083/jcb.202003149
Zhuo, W., M. Sun, K. Wang, L. Zhang, K. Li, D. Yi, M. Li, Q. Sun, X. Ma, W. Liu, et al. 2022. m6Am methyltransferase PCIF1 is essential for aggressiveness of gastric cancer cells by inhibiting TM9SF1 mRNA translation. *Cell Discov.* 8:48. https://doi.org/10.1038/s41421-022-00395-1

JCB

Supplemental material

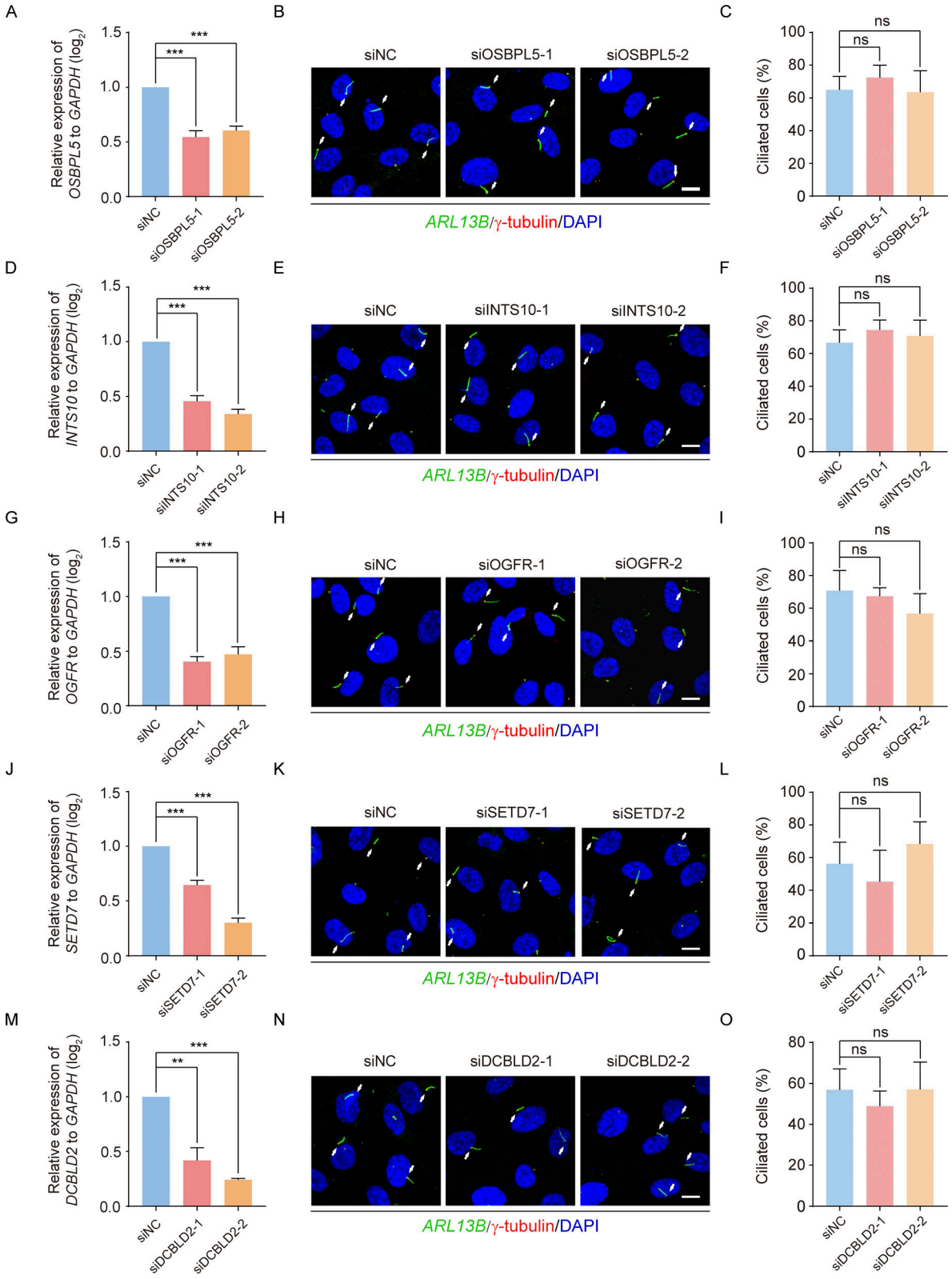

Figure S1. **The effect of *OSBPL5*, *NTS10*, *OGFR*, *SETD7*, and *DCBLD2* knockdown on ciliation.** RPE-1 cells transfected with the indicated siRNAs for 48 h were treated with serum starvation for another 24 h and then subjected to RT-qPCR analysis or immunofluorescence. **(A, D, G, J, and M)** RT-qPCR analysis of the related mRNAs of the five genes depleted RPE-1 cells. *GAPDH* is the internal control. **(B, E, H, K, and N)** Immunofluorescence images of RPE-1 cells with anti-ARL13B (green) and γ-tubulin (red) antibodies. DNA was stained with DAPI (blue). Cilia were indicated by white arrows. Scale bar, 10 µm. **(C, F, I, L, and O)** Quantification analysis of the percentage of ciliated cells). Data are means ± SD of three independent experiments. Student's *t* test was performed. ns, not significant.

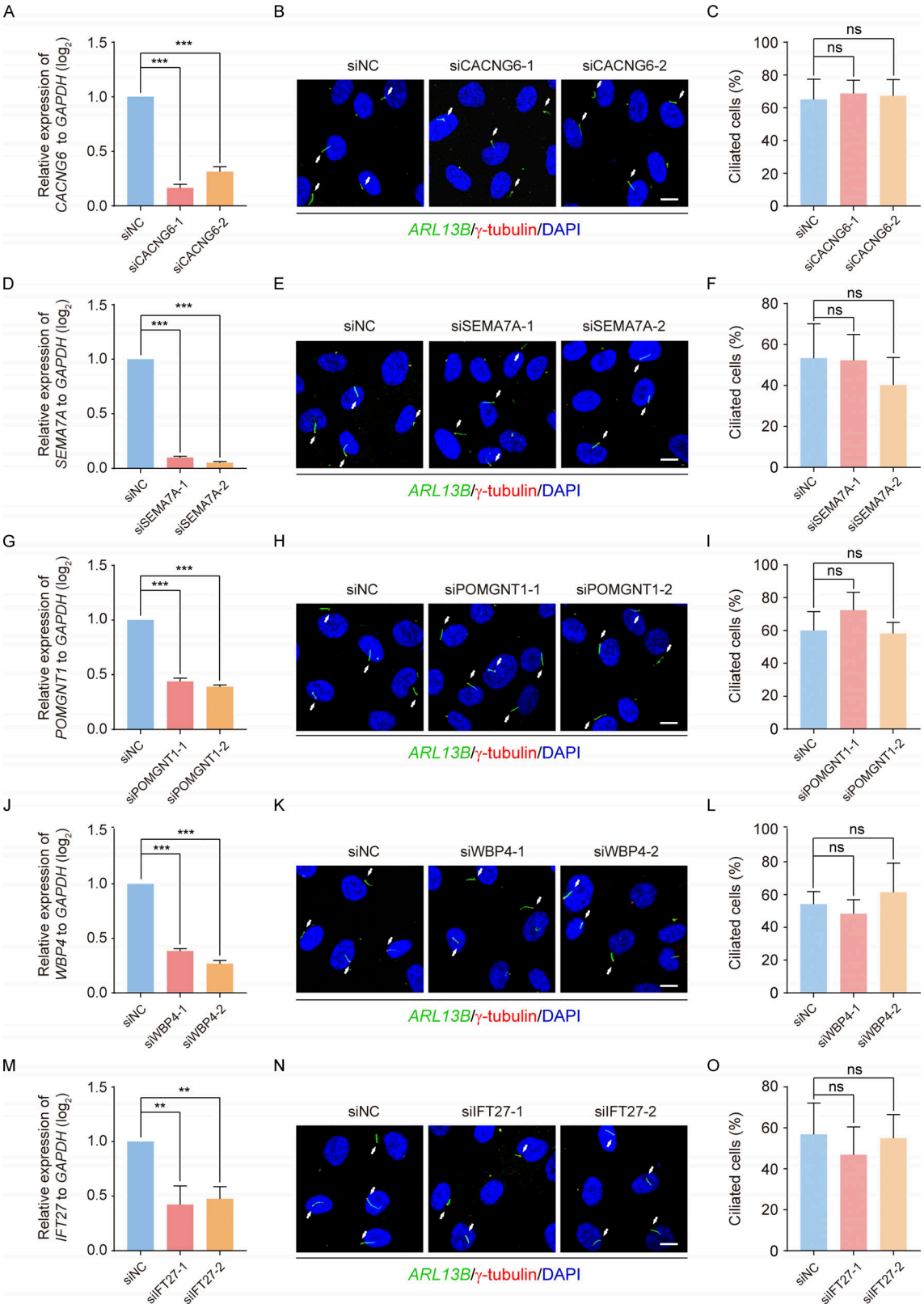

Figure S2. **The effect of *CACNG6*, *SEMA7A*, *POMGNT1*, *WBP4*, and *IFT27* genes knockdown on ciliation.** RPE-1 cells transfected with the indicated siRNAs for 48 h were treated with serum starvation for another 24 h and then subjected to RT-qPCR analysis or immunofluorescence. **(A, D, G, J, and M)** RT-qPCR analysis of the related mRNAs of the five genes depleted RPE-1 cells. *GAPDH* is the internal control. **(B, E, H, K, and N)** Immunofluorescence images of RPE-1 cells with anti-ARL13B (green) and γ-tubulin (red) antibodies. DNA was stained with DAPI (blue). Cilia were indicated by white arrows. Scale bar, 10 µm. **(C, F, I, L, and O)** Quantification analysis of the percentage of ciliated cells. Data are means ± SD of three independent experiments. Student's *t* test was performed. ns, not significant.

Provided online are Table S1, Table S2, Table S3, Table S4, and Table S5. Table S1 shows the analysis of TMT proteomics. Table S2 shows significant hit proteins for siPCIF1-1 versus its control. Table S3 shows significant hit proteins for siPCIF1-2 versus its control. Table S4 shows sequences of siRNAs. Table S5 shows sequences of primers used in this study.